Experimental verification of soliton-like pulse-shaping mechanisms in passively mode-locked VECSELs

Martin Hoffmann*, Oliver D. Sieber, Deran J. H. C. Maas, Valentin J. Wittwer, Matthias Golling, Thomas Südmeyer, and Ursula Keller

Department of Physics, Institute of Quantum Electronics, ETH Zurich, 8093 Zurich, Switzerland
**mh@phys.ethz.ch*

Abstract: We present a detailed experimental study on the influence of dispersion on the pulse formation in passively modelocked vertical-external-cavity surface-emitting lasers (VECSELs). We have demonstrated that the shortest pulse duration requires slightly positive dispersion to balance the nonlinear phase shift induced by strong semiconductor gain and absorber saturation. This is in contrast to soliton modelocking in ion-doped solid-state lasers – but similarities remain and will be discussed. Our results are in good qualitative agreement with numerical simulations and confirm the quasi-soliton modelocking mechanism of ultrafast VECSELs.

OCIS codes: (140.7260) Vertical cavity surface emitting lasers; (140.4050) Mode-locked lasers.

References and links

1. M. Kuznetsov, F. Hakimi, R. Sprague, and A. Mooradian, "High-Power (>0.5-W CW) Diode-Pumped Vertical-External-Cavity Surface-Emitting Semiconductor Lasers with Circular TEM00 Beams," IEEE Photon. Technol. Lett. **9**(8), 1063–1065 (1997).
2. U. Keller, K. J. Weingarten, F. X. Kärtner, D. Kopf, B. Braun, I. D. Jung, R. Fluck, C. Hönninger, N. Matuschek, and J. Aus der Au, "Semiconductor saturable absorber mirrors (SESAMs) for femtosecond to nanosecond pulse generation in solid-state lasers," IEEE J. Sel. Top. Quantum Electron. **2**(3), 435–453 (1996).
3. U. Keller, D. A. B. Miller, G. D. Boyd, T. H. Chiu, J. F. Ferguson, and M. T. Asom, "Solid-state low-loss intracavity saturable absorber for Nd:YLF lasers: an antiresonant semiconductor Fabry-Perot saturable absorber," Opt. Lett. **17**(7), 505–507 (1992).
4. S. Hoogland, S. Dhanjal, A. C. Tropper, J. S. Roberts, R. Haring, R. Paschotta, F. Morier-Genoud, and U. Keller, "Passively mode-locked diode-pumped surface-emitting semiconductor laser," IEEE Photon. Technol. Lett. **12**(9), 1135–1137 (2000).
5. K. G. Wilcox, Z. Mihoubi, G. J. Daniell, S. Elsmere, A. Quarterman, I. Farrer, D. A. Ritchie, and A. Tropper, "Ultrafast optical Stark mode-locked semiconductor laser," Opt. Lett. **33**(23), 2797–2799 (2008).
6. P. Klopp, U. Griebner, M. Zorn, A. Klehr, A. Liero, M. Weyers, and G. Erbert, "Mode-locked InGaAs-AlGaAs disk laser generating sub-200-fs pulses, pulse picking and amplification by a tapered diode amplifier," Opt. Express **17**(13), 10820–10834 (2009).
7. A. H. Quarterman, K. G. Wilcox, V. Apostolopoulos, Z. Mihoubi, S. P. Elsmere, I. Farrer, D. A. Ritchie, and A. Tropper, "A passively mode-locked external-cavity semiconductor laser emitting 60-fs pulses," Nat. Photonics **3**(12), 729–731 (2009).
8. A. Aschwanden, D. Lorenser, H. J. Unold, R. Paschotta, E. Gini, and U. Keller, "2.1-W picosecond passively mode-locked external-cavity semiconductor laser," Opt. Lett. **30**(3), 272–274 (2005).
9. B. Rudin, A. Rutz, M. Hoffmann, D. J. H. C. Maas, A.-R. Bellancourt, E. Gini, T. Südmeyer, and U. Keller, "Highly efficient optically pumped vertical-emitting semiconductor laser with more than 20 W average output power in a fundamental transverse mode," Opt. Lett. **33**(22), 2719–2721 (2008).
10. U. Keller, and A. C. Tropper, "Passively modelocked surface-emitting semiconductor lasers," Phys. Rep. **429**(2), 67–120 (2006).
11. D. J. H. C. Maas, A.-R. Bellancourt, B. Rudin, M. Golling, H. J. Unold, T. Südmeyer, and U. Keller, "Vertical integration of ultrafast semiconductor lasers," Appl. Phys. B **88**(4), 493–497 (2007).
12. V. J. Wittwer, B. Rudin, D. J. H. C. Maas, Y. Barbarin, M. Hoffmann, M. Golling, T. Südmeyer, and U. Keller, "Modelocked Integrated External-Cavity Surface Emitting Laser (MIXSEL) generates 660 mW average power in 23-ps pulses at 3 GHz repetition rate," ASSP Conference 2010 (2010).
13. A.-R. Bellancourt, D. J. H. C. Maas, B. Rudin, M. Golling, T. Südmeyer, and U. Keller, "Modelocked integrated external-cavity surface emitting laser," IET Optoelectron. **3**(2), 61–72 (2009).

#125661 - $15.00 USD Received 18 Mar 2010; revised 22 Apr 2010; accepted 25 Apr 2010; published 29 Apr 2010

14. I. Young, E. Mohammed, J. Liao, S. Alexandra Kern Palermo, B. Block, M. Reshotko, and P. Chang, "Optical I/O Technology for Tera-Scale Computing," IEEE International Solid-State Circuits Conference 2009 (2009).
15. D. Huang, E. A. Swanson, C. P. Lin, J. S. Schuman, W. G. Stinson, W. Chang, M. R. Hee, T. Flotte, K. Gregory, C. A. Puliafito, and J. G. Fujimoto, "Optical coherence tomography," Science **254**(5035), 1178–1181 (1991).
16. H. R. Telle, G. Steinmeyer, A. E. Dunlop, J. Stenger, D. H. Sutter, and U. Keller, "Carrier-envelope offset phase control: A novel concept for absolute optical frequency measurement and ultrashort pulse generation," Appl. Phys. B **69**(4), 327–332 (1999).
17. T. Udem, R. Holzwarth, and T. W. Hänsch, "Optical frequency metrology," Nature **416**(6877), 233–237 (2002).
18. S. A. Diddams, T. Udem, J. C. Bergquist, E. A. Curtis, R. E. Drullinger, L. Hollberg, W. M. Itano, W. D. Lee, C. W. Oates, K. R. Vogel, and D. J. Wineland, "An optical clock based on a single trapped 199Hg+ ion," Science **293**(5531), 825–828 (2001).
19. D. J. H. C. Maas, A. R. Bellancourt, M. Hoffmann, B. Rudin, Y. Barbarin, M. Golling, T. Südmeyer, and U. Keller, "Growth parameter optimization for fast quantum dot SESAMs," Opt. Express **16**(23), 18646–18656 (2008).
20. I. D. Jung, F. X. Kärtner, L. R. Brovelli, M. Kamp, and U. Keller, "Experimental verification of soliton mode locking using only a slow saturable absorber," Opt. Lett. **20**(18), 1892–1894 (1995).
21. F. X. Kärtner, I. D. Jung, and U. Keller, "Soliton Mode-Locking with Saturable Absorbers," IEEE J. Sel. Top. Quantum Electron. **2**(3), 540–556 (1996).
22. R. Paschotta, R. Häring, A. Garnache, S. Hoogland, A. C. Tropper, and U. Keller, "Soliton-like pulse-shaping mechanism in passively mode-locked surface-emitting semiconductor lasers," Appl. Phys. B **75**(4-5), 445–451 (2002).
23. U. Keller, "Ultrafast solid-state lasers," in Landolt-Börnstein. Laser Physics and Applications. Subvolume B: Laser Systems. Part I., G. Herziger, H. Weber, and R. Proprawe, eds. (Springer Verlag, Heidelberg, 2007), pp. 33–167.
24. F. Gires, and P. Tournois, "Interferometre utilisable pour la compression d'impulsions lumineuses modulees en frequence," Acad. Sci., Paris, C. R. **258**, 6112–6115 (1964).
25. A. Gosteva, M. Haiml, R. Paschotta, and U. Keller, "Noise-related resolution limit of dispersion measurements with white-light interferometers," J. Opt. Soc. Am. B 22, 1868-1875 (2005).
26. D. Lorenser, H. J. Unold, D. J. H. C. Maas, A. Aschwanden, R. Grange, R. Paschotta, D. Ebling, E. Gini, and U. Keller, "Towards Wafer-Scale Integration of High Repetition Rate Passively Mode-Locked Surface-Emitting Semiconductor Lasers," Appl. Phys. B **79**(8), 927–932 (2004).
27. D. J. H. C. Maas, B. Rudin, A.-R. Bellancourt, D. Iwaniuk, S. V. Marchese, T. Südmeyer, and U. Keller, "High precision optical characterization of semiconductor saturable absorber mirrors," Opt. Express **16**(10), 7571–7579 (2008).
28. G. P. Agrawal, and C. M. Bowden, "Concept of linewidth enhancement factor in semiconductor lasers: its usefulness and limitations," IEEE Photon. Technol. Lett. **5**(6), 640–642 (1993).

1. Introduction

Soon after the first demonstration of a passively modelocked vertical-external-cavity surface-emitting laser (VECSEL [1],) with a semiconductor saturable absorber mirror (SESAM [2,3],) in 2000 [4] their performance has surpassed other ultrafast semiconductor lasers in average power, pulse quality and pulse duration. Without external pulse compression, they offer the shortest pulses directly from a semiconductor laser [5,6], and recently even sub-100 fs pulses have been achieved [7]. Moreover, ultrafast optically pumped VECSELs can generate substantially higher average output powers than other modelocked semiconductor lasers with currently up to 2.1 W in 4.7-ps pulses [8]. The vertical-emitting geometry has a clear power scaling advantage, which has enabled continuous-wave (cw) power of up to 20 W in fundamental transverse mode operation [9]. Many different operation wavelengths can be easily achieved with band gap engineering and a more detailed review is given in [10]. Furthermore, the SESAM and the VECSEL gain structure can be integrated into a single semiconductor structure, which is referred to as modelocked integrated external-cavity surface emitting laser (MIXSEL [11],). So far, MIXSELs have generated an average power of up to 660 mW in 23-ps pulses and operated at repetition rates up to 10 GHz [12]. The compactness and the simplicity of the MIXSEL platform appears well-suited for cost-efficient mass production [13] and large-scale applications such as optical interconnects or optical clocking of future high frequency multi-core microprocessors [14].

Many other applications such as broadband continuum generation for illumination and optical coherence tomography [15], self-referenced frequency combs [16] for metrology applications [17,18], and biomedical imaging need high power femtosecond pulses.

#125661 - $15.00 USD Received 18 Mar 2010; revised 22 Apr 2010; accepted 25 Apr 2010; published 29 Apr 2010

Therefore, one of the next milestones in ultrafast VECSELs and MIXSELs is the power scaling in the femtosecond regime. To date femtosecond VECSELs have generated only limited average output powers well below 100 mW. Femtosecond high-power pulse generation will require a more detailed understanding of the pulse forming mechanism in modelocked VECSELs and further optimization of the experimental key parameters such as dispersion and SESAM recovery time [19].

Motivated by the successful soliton modelocking model [20,21] in SESAM modelocked ion-doped solid-state lasers, we have performed a theoretical study on soliton-like pulse-shaping mechanism for SESAM-modelocked VECSELs [22]. For soliton modelocking in ion-doped solid-state lasers self-phase modulation (SPM) $\varphi(t) = kn_2 I(t)$ and negative group delay dispersion (GDD) is balanced to form soliton pulses (with sech^2-shaped temporal profile), where k is the wave number in vacuum, n_2 the nonlinear refractive index and $I(t)$ the pulse intensity. For normal materials the n_2 is positive and soliton formation then requires negative GDD. In the femtosecond to few picosecond domain this pulse formation process becomes dominant and the SESAM only starts and stabilizes this pulse formation process. This relaxes the requirements on the SESAM parameters. Passive modelocking at gigahertz repetition rates typically has negligible SPM and therefore soliton modelocking becomes less effective at these high pulse duty cycles and correspondingly lower peak powers. Furthermore, in contrast to ion-doped solid-state lasers semiconductor lasers exhibit strong dynamic gain saturation [23]. The combination of both the nonlinear phase shift introduced by the dynamic gain saturation and the fast absorber saturation leads mathematically to a similar effect as SPM but with a negative n_2. We therefore referred to this modelocking regime in VECSELs as quasi-soliton modelocking [22] for which in mathematical analogy to the soliton modelocking model the interplay of a nonlinear phase shift with *positive* intra-cavity GDD becomes the dominant pulse forming mechanism. Thus, this nonlinear phase shift is not based on SPM but is induced by significant VECSEL gain and SESAM saturation. The combination of both effects behaves approximately like a negative SPM material (i.e. negative n_2). Therefore, soliton-like pulse formation is obtained with positive instead of negative GDD and this pulse-shaping theory is referred to as quasi-soliton modelocking. In [22], however, only a qualitative experimental agreement could be found, since various important parameters were changed simultaneously during the experiments.

Here, we present the results of the first systematic experimental investigation of the influence of intra-cavity GDD on the pulse duration for SESAM modelocked VECSELs. For this study, we developed a versatile new type of dispersive mirror based on a hybrid semiconductor/dielectric coating approach. It allowed us to discretely vary the overall intra-cavity GDD between -14000 fs^2 and 18000 fs^2 by simply introducing different dispersive mirrors into the laser cavity. Our experiments confirm the quasi-soliton pulse-shaping mechanism for VECSELs, show good qualitative agreement with numerical simulations and confirm that indeed positive GDD is required for the shortest pulses. In addition, we found an additional benefit with a high tolerance in positive GDD values for the pulse duration.

2. Design of hybrid semiconductor/dielectric coating dispersive mirrors

In order to experimentally control the GDD of our modelocked VECSELs, we developed a new type of dispersive mirrors. We produced a set of different mirrors with GDD values ranging between -7000 fs^2 to 9000 fs^2 for a single reflection. We based the devices on a standard Gires-Tournois interferometer (GTI [24],) design [see Fig. 1(a)]. A standard GTI design consists of a highly reflective (HR) and a partially reflective (PR) mirror section, which are separated by a spacer layer. An incoming beam is typically sent at nearly perpendicular incidence onto the PR section. The transmitted light that enters the spacer layer will be reflected by the HR section, which ideally has a reflectivity of 100%. In the case of no

#125661 - $15.00 USD Received 18 Mar 2010; revised 22 Apr 2010; accepted 25 Apr 2010; published 29 Apr 2010

losses, the GTI will reflect everything but with a wavelength-dependent phase-shift that can generate either positive or negative GDD. The amount of GDD depends on the wavelength, the reflectivity of the PR mirror section, the spacer material and the spacer thickness.

In Fig. 2(a), we show the calculated dispersion for a GTI consisting of a standard HR mirror section [realized by a GaAs/AlAs distributed Bragg reflector (DBR)] and the Fresnel reflection of the spacer/air interface as PR mirror section. We chose two different spacer materials, GaAs and fused silica, and plotted the resulting GDD as a function of the spacer thickness for a center wavelength of 960 nm. For the GaAs spacer, we can obtain sufficiently large values for the GDD, however it would require very precise layer thickness control. For example, for a design value of 4500 fs^2, a difference in spacer-thickness of 1 nm would correspond to an error in GDD of ≈223 fs^2. This accuracy is difficult to achieve with standard processing methods.

In comparison, fused silica as a spacer material provides a much smoother GDD dependence on the material thickness. In addition, fused silica can easily be deposited on multiple semiconductor samples with different and accurately controllable thicknesses using plasma enhanced chemical vapor deposition (PECVD). The only drawback is the limited amount of GDD that we can obtain for typical layer thicknesses below 1 µm.

Because fused silica or GaAs spacer materials did not provide the required dispersion properties, we used a hybrid approach for our dispersive mirror design, which benefits from the advantages of both materials. Its main part consists of a bottom DBR and a 3.1-µm thick GaAs layer, which can provide a sufficiently large amount of dispersion (in the order of 10^4 fs^2). For the fine adjustment of the final GDD, we insert an anti-reflective (AR) section on the top, and add an additional layer of fused silica. The thickness of this fused silica layer needs to be controlled very accurately in order to obtain a specific value for the GDD of the final dispersive mirror. The AR section consists of a 10-layer AlAs/GaAs system to reduce internal reflections between the 3.1-µm thick GaAs layer and the fused silica layer to less than 0.1% for the entire wavelength range from 950 to 970 nm.

The GDD of such a dispersive element is plotted as a function of the fused silica layer thickness in Fig. 2(b) for a wavelength of 960 nm. The final design is shown in Fig. 1(b).

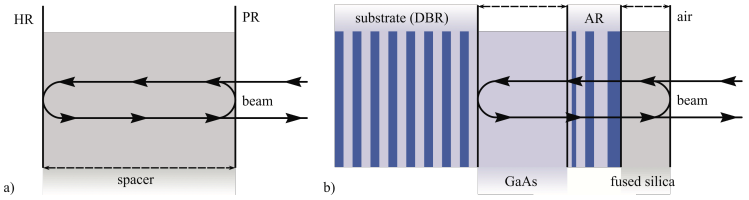

Fig. 1. (a) Basic principle of a GTI, consisting of a high reflector (HR), a spacer layer and a partial reflector (PR). (b) Our dispersive mirror design, consisting of a GaAs/AlAs DBR as the HR, the top air interface as the PR and the total spacer layer formed by the GaAs, anti-reflection (AR) and the fused silica (FS) layers. The GaAs layer was chosen to be 3.1 µm thick whereas the fused silica layer thickness was varied to adjust the final dispersion of the dispersive mirror device.

We grew the semiconductor part of the design using molecular beam epitaxy (MBE) on a 650 µm GaAs wafer (using a VEECO GEN III MBE of the ETH FIRST lab). After cleaving the wafer into 3x3 mm^2 pieces, we added the fused silica coatings with different thicknesses to obtain a set of dispersive mirrors. The thicknesses of the fused silica layers on the individual samples ranged from 80 nm to 350 nm which correspond to GDD values between –7000 fs^2 and 9000 fs^2 [see Fig. 2(c)].

The GDD curves for some of the fabricated devices are plotted in Fig. 2(c) as a function of the wavelength. The measurement data is plotted as dots and a corresponding spline interpolation is plotted as a solid line for each of the dispersive mirrors. Figure 2(d) shows the comparison of our GDD simulation (red line) with the GDD measurement results (points with

#125661 - $15.00 USD Received 18 Mar 2010; revised 22 Apr 2010; accepted 25 Apr 2010; published 29 Apr 2010

a black line spline fit) for one of our devices, in this case for that with a fused silica layer thickness of 285 nm. All GDD measurements were done with a home-built GDD measurement setup based on white-light interferometry [25].

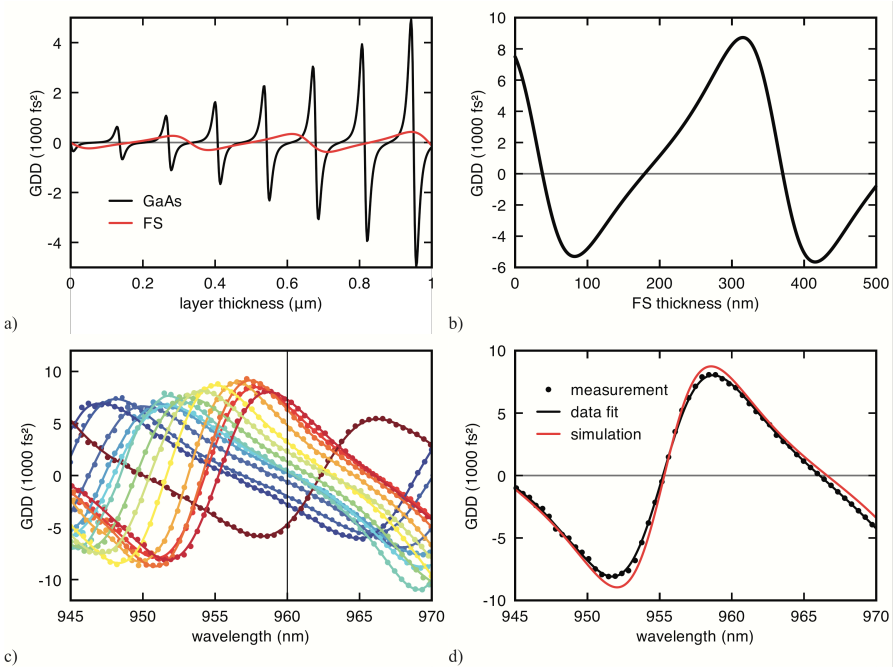

Fig. 2. (a) Comparison of two different GTI spacer materials. The GaAs GDD range is much larger compared to fused silica, however, the slope is not as linear. (b) For the dispersive mirror design from Fig. 1(b) the GDD as a function of the fused silica layer thickness is plotted. (c) Measurement (dots) and a spline interpolation (lines) of the wavelength dependent GDD for some of our fabricated dispersive mirrors. (d) Comparison of the measured GDD (dots) and the corresponding spline fit (black line) with our GDD simulation (red line) for a dispersive mirror with a fused silica layer thickness of 285 nm.

3. Experimental laser setup

For our experiment we used a standard z-shaped cavity (Fig. 3) with an output coupler, an optically pumped VECSEL gain-structure, one of the dispersive mirrors, a SESAM and a 20-µm thick etalon for wavelength tunability. To change the overall GDD of the laser cavity, we use the set of dispersive mirrors as described in Section 2. Thus, the total intra-cavity GDD can be changed without changing the emission wavelength which can be controlled by the 20-µm thick fused silica etalon.

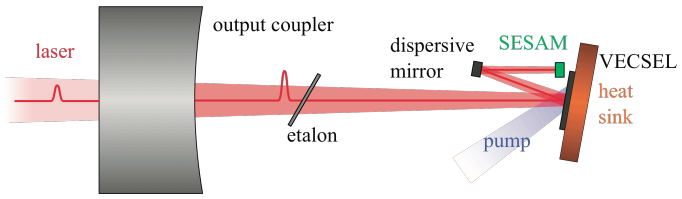

Fig. 3. Laser cavity, consisting of an output coupler, an etalon for wavelength tuning, the VECSEL gain structure, a dispersive mirror and a SESAM.

The VECSEL was grown in the FIRST clean room facility at ETH Zurich using metal-organic vapor-phase epitaxy (MOVPE i.e. a AIXTRON AIX 200/4 MOVPE) with a design similar to [8]. The VECSEL contains an AlAs/AlGaAs DBR which reflects both the laser and

#125661 - $15.00 USD Received 18 Mar 2010; revised 22 Apr 2010; accepted 25 Apr 2010; published 29 Apr 2010

the pump wavelength using a super lattice mirror structure design. The calculated reflectivity for the laser wavelength at 10° angle of incidence is >99.95% and for the pump radiation at an angle of incidence of 45° it is >99.5%. The active region of the VECSEL consists of seven InGaAs quantum wells (QWs) with a thickness of 5 nm, placed at the peaks of the standing wave pattern of the electric field inside the VECSEL structure. The QWs are spaced by GaAs spacer layers which also serve as absorbing medium for the pump radiation. From these spacer layers the excited carriers can drift into the QWs. On top of the active region there is an AR-section which controls the field enhancement in the gain region.

Self-starting and reliable modelocking is achieved with a quantum-dot (QD) SESAM with moderate saturation fluence [19]. It consists of an AlAs/GaAs DBR, a single InAs QD saturable absorber layer which is centered at a maximum of the standing wave pattern of the electric field and several AlAs/GaAs layers on top of the structure to control the field enhancement. The SESAM was grown using MBE at the FIRST clean room facility at ETH in Zurich and it has a resonant design similar to the one described in [26]. We measured its nonlinear reflectivity with a homebuilt high dynamic range setup [27], which was driven by 180-fs pulses at 956 nm from a commercial 80-MHz repetition rate Ti:sapphire laser. The measured saturation fluence is 4.2 μJ/cm^2, the modulation depth 1.3%, and the nonsaturable losses are < 1%. Due to the resonant design, both the modulation depth and the saturation fluence are wavelength dependent. With increasing wavelength, the saturation fluence increases and the modulation depth decreases.

The laser mode radius on the VECSEL was ≈90 μm and on the SESAM ≈45 μm. The VECSEL gain structure was pumped optically using an 808 nm diode laser at a pumping angle of about 45°. The output coupling mirror had a radius of curvature of 38 mm and a reflectivity of 99.3% (i.e. an output coupling of 0.7%). The temperature of the VECSEL heat sink was set to 5°C. The typical output power was about 30 mW for all GDD dependent measurements.

In Fig. 4, we show the autocorrelation and the optical spectrum of the pulses with the shortest pulse duration of 1.52 ps with 30 mW of average output power, at 4.2 GHz repetition rate and with a positive total intra-cavity dispersion of 5300 fs^2. The FWHM spectral width of the pulses was 0.86 nm, resulting in a time bandwidth product (TBP) of 0.43 which is 1.35 times the transform limit of an ideal sech^2 soliton pulse shape.

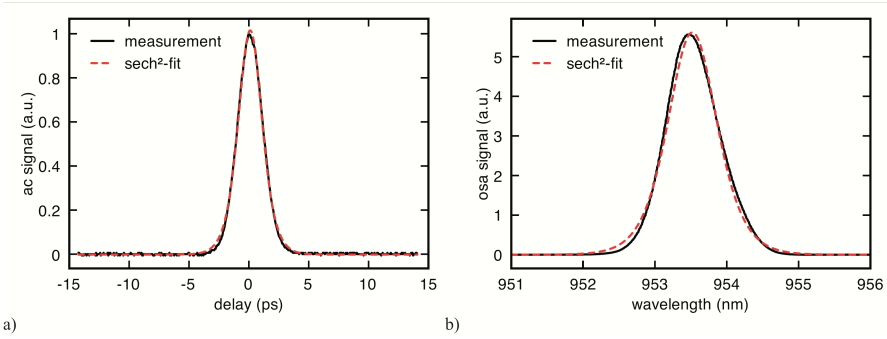

Fig. 4. Measurement of the shortest pulses we obtained during our experimental study. a) Second-harmonic autocorrelation trace with a sech^2-fit showing a pulse duration of 1.52 ps and b) optical spectrum with a measured spectral width of 0.86 nm.

4. GDD dependent results

Both VECSELs and SESAMs provide a significant amount of dispersion (in the range of ± 10^4 fs^2), which strongly depends on the operation wavelength. The typical MBE growth accuracy leads to a relatively large uncertainty, and measurements of the real GDD are needed. Therefore, we first measured the wavelength-dependent GDD of the VECSEL, the SESAM and all fabricated dispersive mirrors with our home-built GDD measurement setup

#125661 - $15.00 USD Received 18 Mar 2010; revised 22 Apr 2010; accepted 25 Apr 2010; published 29 Apr 2010

based on white-light interferometry [25]. An example of the obtained GDD curves for the whole cavity, as well as the individual cavity elements for one specific cavity setup, is given in Fig. 5(a) The GDD of the entire cavity was then determined according to Eq. (1)

$$\mathrm{GDD}_{\mathrm{cavity}} = 2 \cdot \mathrm{GDD}_{\mathrm{VECSEL}} + 2 \cdot \mathrm{GDD}_{\mathrm{dispersive\ mirror}} + \mathrm{GDD}_{\mathrm{SESAM}}, \quad (1)$$

because the laser cavity beam has two passes through the VECSEL and dispersive mirror and only one pass through the SESAM per cavity round trip (see Fig. 3).

For every dispersive mirror we changed the center wavelength of the laser emission using the etalon, tuning the wavelength between 950 nm and 960 nm in increments of 0.5 nm. We determined the optical spectrum, the microwave spectrum, and the autocorrelation (AC) trace using a standard second harmonic generation (SHG) autocorrelator. We took special care during those measurements not to alter other parameters, such as the repetition rate or the pump power, to insure that only the total intra-cavity GDD dependence was investigated. Therefore, we can determine the pulse duration as a function of the total intra-cavity GDD for any given emission wavelength from these measurements because every dispersive mirror has a different wavelength-dependent GDD [Fig. 2(c)].

In Fig. 5(b), the measured pulse duration is given as a function of the total intra-cavity GDD for several different laser wavelengths.

#125661 - $15.00 USD Received 18 Mar 2010; revised 22 Apr 2010; accepted 25 Apr 2010; published 29 Apr 2010

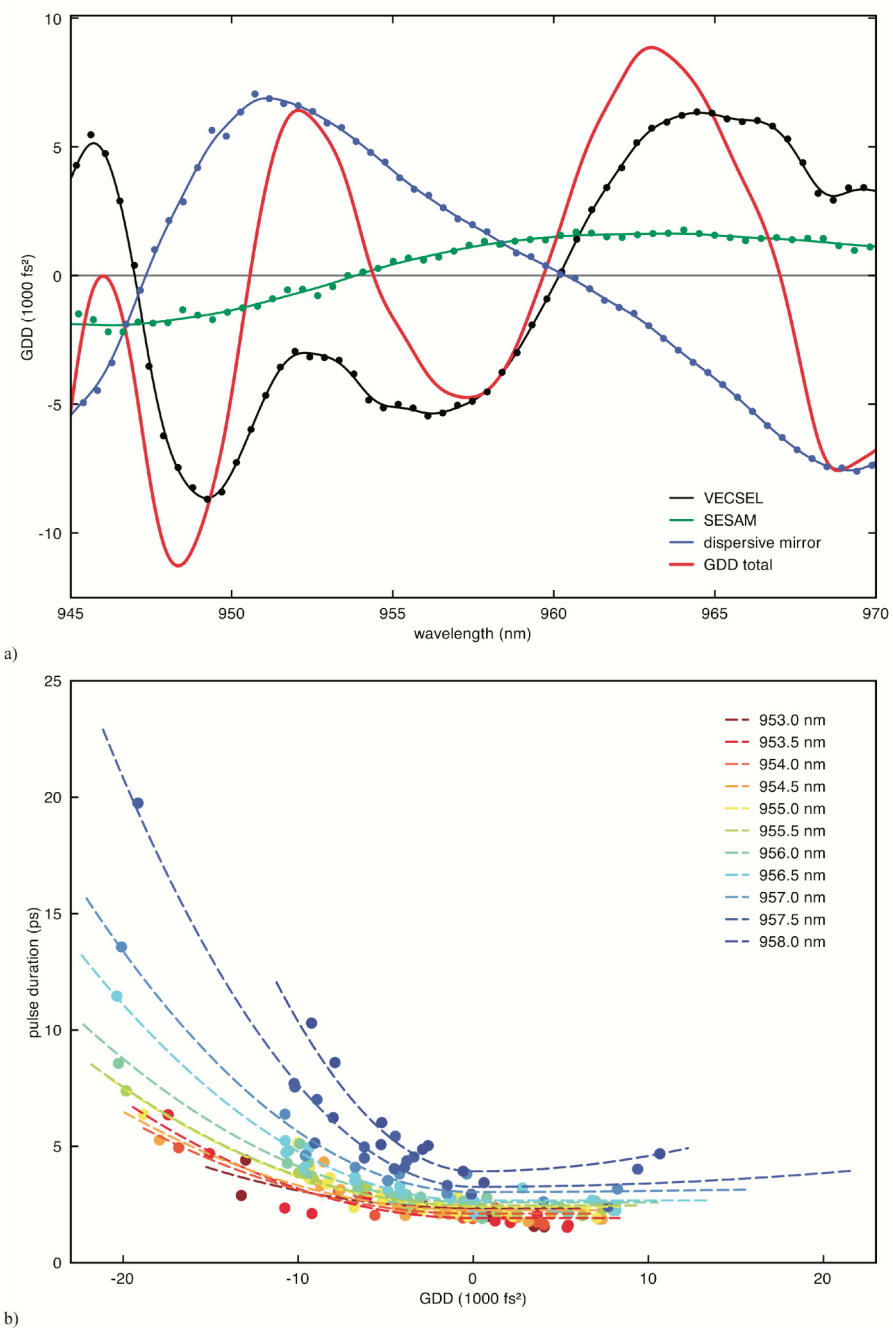

Fig. 5. (a) The wavelength dependent GDD for the individual cavity elements and the total intra-cavity GDD according to Eq. (1). (b) Measured pulse duration as a function of the total intra-cavity GDD for several different laser wavelengths. The measurements are plotted as dots, the lines serve as guides to the eye.

We clearly see that the pulse duration strongly depends on the amount of total intra-cavity GDD. For positive GDD values the pulse duration becomes shorter compared to negative GDD values. The minimum duration is observed at low positive values between 2000 and 6000 fs^2. The pulse duration for a given value of intra-cavity GDD depends strongly on the

#125661 - $15.00 USD Received 18 Mar 2010; revised 22 Apr 2010; accepted 25 Apr 2010; published 29 Apr 2010

operation wavelength, which is mainly due to the resonant SESAM design, which introduces a significant wavelength dependent modulation depth and saturation fluence. This effect, however, is much more pronounced in the negative GDD regime compared to the positive [see Fig. 5(b)].

5. Numerical Simulations

We compared our experimental data with numerical simulations done in MATLAB. We simulated the pulse propagation by implementing numerical iterations of a circulating pulse inside a VECSEL cavity, similar to [22]. Within a cavity round trip the pulse interacts with the cavity elements such as gain, absorber, output coupler and cavity dispersion. These elements are represented by operators either in time or frequency domain. The slowly varying envelope approximation is used to describe the temporal evolution of the pulse shape and fast Fourier transformation (FFT) converts the pulse between the time and the frequency domain. The effects our simulation takes into account are shown in Fig. 6.

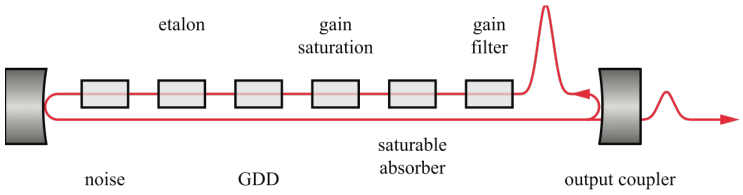

Fig. 6. Numerical simulation model: a pulse circulates in the cavity with all listed effects taken into account either in the time or frequency domain.

The gain filter simulates the optical gain with respect to the center wavelength and the bandwidth. Effects of dynamic saturation of the gain and the absorber are described in the time domain using the differential equation Eq. (2)

$$\frac{\mathrm{d}g(t)}{\mathrm{d}t} = \frac{g_0 - g(t)}{\tau} - g(t)\frac{P(t)}{E_{\mathrm{sat}}}, \tag{2}$$

where $g(t)$ is the wavelength-independent gain, g_0 the small signal gain, τ the recombination time, $P(t)$ the instantaneous power and E_{sat} the saturation energy. For the gain we have a positive small signal gain $g_0 > 0$ while for the saturable absorber we used a negative approximated value of $g_0 = -\Delta R/2$, with ΔR the modulation depth. By Kramers-Kronig relations, the saturation of the gain and the absorber also implies a change of the real part of the refractive index which results in a nonlinear phase change. The relation between saturation and phase change is given by Eq. (3)

$$\Delta\varphi(t) = -\frac{\alpha}{2}\Delta g(t), \tag{3}$$

where α is the empiric line width enhancement factor [28]. The values we use in our simulation were $\alpha_{\mathrm{absorber}} = 2$ and $\alpha_{\mathrm{gain}} = 3$. The GDD is included in the model by applying Eq. (4)

$$\phi(\omega) = \frac{1}{2}\mathrm{GDD}(\omega - \omega_0)^2 \tag{4}$$

in the frequency domain, where ϕ is the spectral phase and ω_0 the reference frequency. During the simulations we maintained a constant GDD value over the full optical pulse spectrum. With this model we can simulate the pulse build-up from a nW-noise floor which is illustrated in Fig. 7.

#125661 - $15.00 USD Received 18 Mar 2010; revised 22 Apr 2010; accepted 25 Apr 2010; published 29 Apr 2010

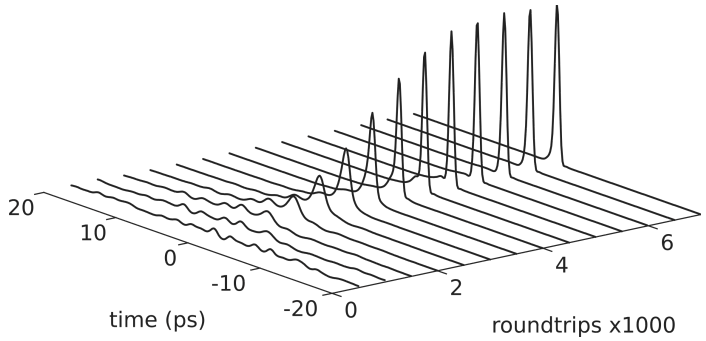

Fig. 7. Pulse build-up from noise, assuming 1 nW noise power. The following parameters for the SESAM were used in the simulation: F_{sat} = 10 μJ/cm^2, ΔR = 0.5%, τ = 20 ps.

Although a pulse build-up from noise is possible, we usually started the simulations with a sech^2-pulse shape, which significantly reduces the number of iterations for a stable solution.

The combination of saturable gain and saturable absorption with negligible intra-cavity SPM results in quasi-soliton modelocking [22] as discussed in Section 1. According to the Kramers-Kronig relation, the saturation directly influences the phase when the laser pulse hits the VECSEL gain structure or the SESAM. The overall phase change is approximately comparable with the phase change from SPM for soliton modelocking as typically observed in ion-doped low repetition rate solid-state lasers. However, the sign is opposite. This behavior is illustrated in Fig. 8(a). For soliton modelocked solid-state lasers, shorter pulses are obtained if SPM is balanced with an appropriate amount of negative cavity GDD. In case of SESAM-modelocked VECSELs, however, the total nonlinear phase change has the opposite sign [Fig. 8(a)] and therefore positive GDD is required for the generation of short pulses. We obtained an asymmetric curve for the pulse duration as a function of the GDD, where positive GDD values are better suited for the generation of short pulses. As one might expect, if saturation effects are neglected, the curve becomes perfectly symmetric which also was reproduced using our theoretical model [Fig. 8(b)].

In comparison to our experimental results our simulations give a good qualitative agreement [see Fig. 8(b) and 8(d)]. For the simulation parameters we used the experimental values from Section 3 and we assumed a gain bandwidth $\Delta\lambda_{gain}$ = 10 nm, $F_{sat,gain}$ = 500 μJ/cm^2, τ_{gain} = 3 ns and $\tau_{absorber}$ = 8 ps. According to our simulations these assumed parameters only have a small influence on the pulse duration. In Fig. 8(d), the measurement results for an emission wavelength of 956 nm are shown together with the corresponding simulation, and in Fig. 8(b) for 957 nm. We clearly see that positive GDD values are favored over negative ones to achieve short pulse durations. This also verifies that the presumed modelocking mechanism for SESAM-modelocked VECSELs is indeed very well described by the quasi-soliton modelocking model.

#125661 - $15.00 USD Received 18 Mar 2010; revised 22 Apr 2010; accepted 25 Apr 2010; published 29 Apr 2010

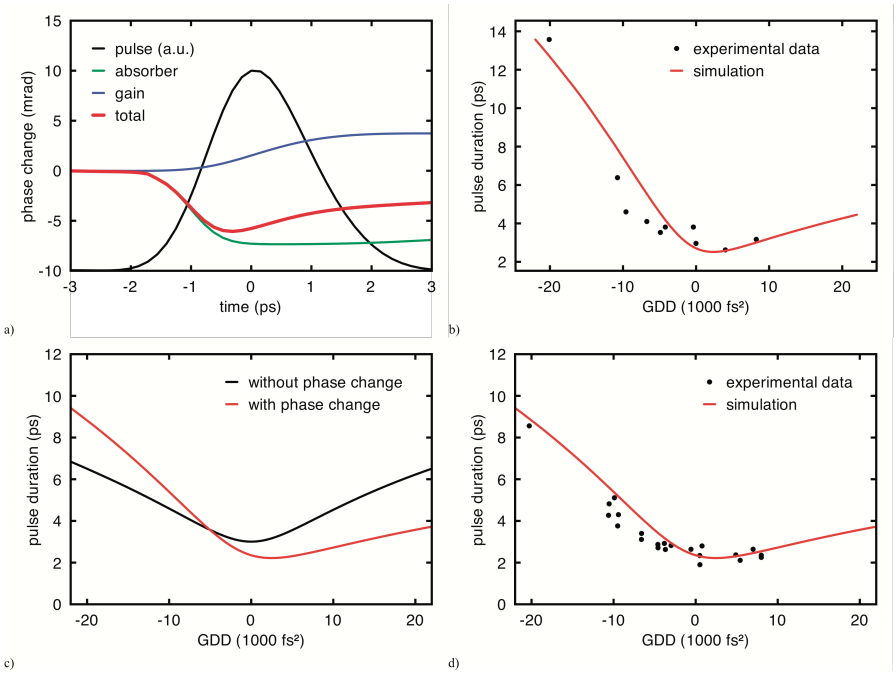

Fig. 8.(a) Time dependent phase change for a given intra-cavity pulse due to the saturation of the absorber, the gain and the sum of the two effects. (c) A comparison between two different simulations, where saturation effects of the VECSEL and the SESAM are taken into account using $\alpha \neq 0$ (red line) and where they are not with $\alpha = 0$ (black line). (b) and (d) Comparison between our theoretical model (red line) and our experimental results (dots) at a center wavelength of 956 nm (d) and 957 nm (b), respectively.

6. Discussion and conclusion

We present the first detailed experimental analysis of the influence of intra-cavity GDD on the pulse duration for passively modelocked VECSELs. In order to be able to change the intra-cavity GDD without changing the laser wavelength we developed a versatile dispersive mirror based on a hybrid semiconductor/dielectric coating approach. Using these devices in our experiments, we confirm that negative GDD results in significantly longer pulses compared to positive GDD. Thus, operation in the low positive GDD regime is ideal for the generation of the shortest pulses. Furthermore, the influence of positive GDD is much reduced compared to negative GDD, resulting in a more relaxed tolerance on the growth accuracy in that regime. The experimentally observed characteristics could also be reproduced in our simulations based on the quasi-soliton theory. We found a good qualitative agreement of the experimental results with our simulations which not only confirms the simplified theory, but also allows for predictions on the pulse duration for specific SESAM-VECSEL combinations. We can now adjust SESAM and VECSEL designs to push the total intra-cavity GDD to slightly positive values. We believe that together with optimized SESAM recovery dynamics and improved gain bandwidth engineering it will be possible to demonstrate power scaling in the femtosecond pulse generation regime as well.

Acknowledgement

This work was supported by ETH Zurich with the FIRST clean room facility and was financed by the Intel Corporation through a university sponsored research agreement, by the Swiss Confederation Program Nano-Tera.ch, which was scientifically evaluated by the SNSF and by the European Community's Seventh Framework Program FAST-DOT under grant agreement 224338.

#125661 - $15.00 USD Received 18 Mar 2010; revised 22 Apr 2010; accepted 25 Apr 2010; published 29 Apr 2010